ACS APPLIED MATERIALS & INTERFACES

www.acsami.org

Research Article

Importance of Electric-Field-Independent Mobilities in Thick-Film Organic Solar Cells

Carr Hoi Yi Ho,* Yusen Pei, Yunpeng Qin, Chujun Zhang, Zhengxing Peng, Indunil Angunawela, Austin L. Jones, Hang Yin, Hamna F. Iqbal, John R. Reynolds, Kenan Gundogdu, Harald Ade, Shu Kong So, and Franky So*

Cite This: *ACS Appl. Mater. Interfaces* 2022, 14, 47961−47970

Read Online

ACCESS | Metrics & More | Article Recommendations | Supporting Information

ABSTRACT: In organic solar cells (OSCs), a thick active layer usually yields a higher photocurrent with broader optical absorption than a thin active layer. In fact, a ∼300 nm thick active layer is more compatible with large-area processing methods and theoretically should be a better spot for efficiency optimization. However, the bottleneck of developing high-efficiency thick-film OSCs is the loss in fill factor (FF). The origin of the FF loss is not clearly understood, and there a direct method to identify photoactive materials for high-efficiency thick-film OSCs is lacking. Here, we demonstrate that the mobility field-dependent coefficient is an important parameter directly determining the FF loss in thick-film OSCs. Simulation results based on the drift−diffusion model reveal that a mobility field-dependent coefficient smaller than 10^{-3} $(V/cm)^{-1/2}$ is required to maintain a good FF in thick-film devices. To confirm our simulation results, we studied the performance of two ternary bulk heterojunction (BHJ) blends, PTQ10:N3:$PC_{71}BM$ and PM6:N3:$PC_{71}BM$. We found that the PTQ10 blend film has weaker field-dependent mobilities, giving rise to a more balanced electron−hole transport at low fields. While both the PM6 blend and PTQ10 blend yield good performance in thin-film devices (∼100 nm), only the PTQ10 blend can retain a FF = 74% with an active layer thickness of up to 300 nm. Combining the benefits of a higher J_{SC} in thick-film devices, we achieved a PCE of 16.8% in a 300 nm thick PTQ10:N3:$PC_{71}BM$ OSC. Such a high FF in the thick-film PTQ10 blend is also consistent with the observation of lower charge recombination from light-intensity-dependent measurements and lower energetic disorder observed in photothermal deflection spectroscopy.

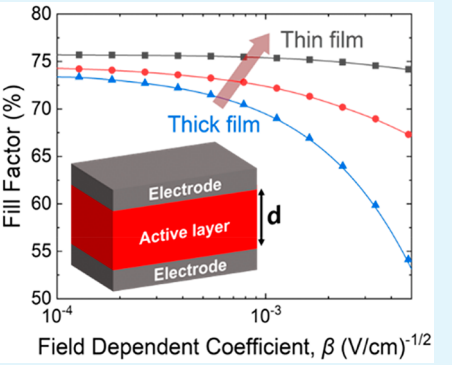

KEYWORDS: *organic photovoltaic, fill factor, thick film, mobility, field dependence, electric field*

Downloaded via NORTH CAROLINA STATE UNIV on November 14, 2022 at 15:43:21 (UTC).
See https://pubs.acs.org/sharingguidelines for options on how to legitimately share published articles.

1. INTRODUCTION

Organic solar cells (OSCs) have attracted extensive attention in the past decade due to their unique advantages, such as lightweight, low cost, flexibility, semitransparency, and solution-processability.[1] In recent years, tremendous progress in the development of OSCs has been achieved via the design of narrow-band-gap donor and acceptor materials, interface engineering, and novel processing methods. With the rapid development of nonfullerene acceptors (NFAs), single-junction OSCs have achieved power conversion efficiencies (PCEs) over 18%.[2−4] However, the best device performance is often achieved in OSCs with a thin-film active layer of ∼100 nm.[5] In large-scale manufacturing, such thin active layers are difficult to process via scalable roll-to-roll printing methods, the active layer thickness should be at least 300 nm.[6] While increasing the active layer thickness should increase the light harvesting efficiency, it also results in a reduction of the device fill factor (FF).[6] Changes in FF are mainly determined by the competition between charge recombination and charge extraction, which in turn depends on the active layer thickness and charge carrier mobility.[7] In thick-film BHJs, photo-generated free carriers must travel a longer distance to reach the respective electrodes, and given the low mobilities of organic semiconductors, the probability of charge carrier recombination is greater.

To address the FF bottleneck, great efforts have been devoted into material design by fine-tuning the energy levels, molecular packing, and crystallinity to yield efficient charge transport.[8,9] Many thick-film OSCs with PCEs beyond 13% are based on donor polymers with a two-dimensional benzodithiophene, such as PM6 or PM7. For example, the addition of fullerene $PC_{61}BM$ into a PBDB-T-2Cl:BTP-4F host blend resulted in an improved nanoscale phase separation and appropriate domain size that favored efficient charge transport

Received: June 24, 2022
Accepted: September 23, 2022
Published: October 11, 2022

ACS Publications

© 2022 American Chemical Society

via a well-distributed nanofibrillar interpenetrating network while suppressing bimolecular recombination, resulting in a PCE of 14.3% and FF of 67% for a 300 nm thick device.[10] Furthermore, Zhang et al. reported several thick-film OSCs using a ternary blend with two NFAs to form an alloyed acceptor domain, providing an additional channel for enhanced charge carrier transport resulting in a PCE of 14% and a FF of 71% in 300 nm thick cells.[11,12] Attempts have been made to understand the origin of the FF loss in thick-film cells. By establishing a correlation between the electron and hole mobilities in different materials with charge carrier recombination, several reports have pointed out the importance of high charge carrier mobilities for achieving high FF in thick-film OSCs.[6,13−17] However, it is well-known that a high carrier mobility does not guarantee a good OSC device performance in a thick active layer film cell, and an in-depth understanding of the origin of the FF loss is imperative to achieve high-efficiency, thick-film OSCs.[5,18]

Space−charge limited current (SCLC) measurements are a widely employed technique to study charge transport of the photoactive materials used in OSCs. However, in many SCLC data reported in the literature, the presence of traps and the quality of the contacts are overlooked and hence the mobility values determined do not reveal the true nature of electron and hole transport.[19−23] Non-ohmic contacts give rise to charge injection barriers, and the existence of traps make the modeling of the experimental data challenging.[19,24,25] Thus, a good fit to the experimental SCLC data can only be obtained at high electric field, resulting in the overestimation of the mobility values.[26,27] In addition to the above two factors, the electric field dependence of the charge carrier mobilities is another often overlooked parameter in these measurements, which further exacerbates the inaccuracy of the SCLC mobility values, especially when the mobility field dependence is large. In a solar cell, under open-circuit and closed-circuit conditions, the electric field strength across the active layer is small. In thick cells, the electric field is much smaller and hence the accurate determination of charge carrier transport is even more challenging. Therefore, determination of the mobility and its field dependence is crucial to accurately predict the performance of a thick cell.

Herein, we first use device simulation to verify the importance of the mobility field dependence. We then experimentally determine the carrier mobility using SCLC by incorporating the field-dependent coefficient (β) and verify the mobility values under different electric fields using admittance spectroscopy (AS). AS is one of the few techniques to directly measure mobilities under different electric fields.[28,29] With this methodology, we can accurately determine the carrier mobilities at zero field as well as at a different field strength.[28] Because the field-dependent mobility is often ignored in the literature, it is therefore important to take it into the account as well as the zero-field mobilities for thick cells.

To illustrate that the field-dependent mobility is a key factor, we first performed device simulations using different values of the mobility field-dependent coefficient (β) for a nominal mobility of $\mu = 2 \times 10^{-4}$ cm^2 V^{-1} s^{-1} obtained from the literature and found that it is indeed a critical value determining the FF loss in thick-film OSCs.[30,31] A high-efficiency thick-film cell requires photoactive materials with a weak field-dependent mobility. We then characterize the carrier transport properties for two ternary bulk heterojunction (BHJ) blends, PTQ10:N3:PC$_{71}$BM and PM6:N3:PC$_{71}$BM. We found that the PTQ10 blend has a weaker field-dependent carrier transport [$\beta \leq 10^{-3}$ (V/cm)$^{-1/2}$] compared to the PM6 blend, giving rise to a more balanced electron−hole transport in the device. Both blends yield over 16% PCE for devices with an ∼100 nm thick active layer; only the PTQ10:N3:PC$_{71}$BM blend retained a high FF with increasing film thickness. Increasing the PTQ10 blend film thickness from 100 to 300 nm results in a small drop in FF from 77% to 74%, while a similar increase in PM6 blend film thickness results in a large drop in FF from 75% to 50%. Due to a slightly higher short-circuit current density (J_{SC}) in the thick-film PTQ10 cell, there is a slight increase in the PCE of the thick-film cell to 16.8%. Additionally, in the PTQ10 blend devices, we also observed less charge recombination from light-intensity-dependent $J-V$ measurements, low energetic disorder from photothermal deflection spectroscopy measurements, and a more uniform donor polymer vertical phase distribution from secondary-ion mass spectrometry. This work highlights the importance of the electric field dependence of charge carrier mobilities in predicting the performance of OSCs and provides new insights into overcoming the FF bottleneck in thick-film devices relevant for large-scale manufacturing.

2. RESULTS AND DISCUSSION

2.1. Simulation on Device Absorption and Fill Factor.

To the first order, thick-film OSCs should have a low effective internal electric field over the operating range from the open-circuit to short-circuit conditions, and in disordered organic semiconductors, electron and hole mobilities are generally electric-field-dependent and can be described by the Poole−Frenkel model (1) with a field-dependent coefficient β,

$$\mu(F) = \mu_0 \exp(0.89\beta\sqrt{F}) \quad (1)$$

where μ_0 is the zero-field mobility and F is the internal electric field. The electric field intensity affects the charge carrier trapping and detrapping processes, giving rise to the field-dependent mobility. To study the effect of field-dependent mobility, we performed drift−diffusion simulations to determine the effects of the β values and active layer film thicknesses on the device FF for a blend with electron and hole zero-field mobility values of 2×10^{-4} cm^2 V^{-1} s^{-1}, and the results are shown in Figure 1. One striking feature is a large drop in FF with increasing active layer thickness when β is

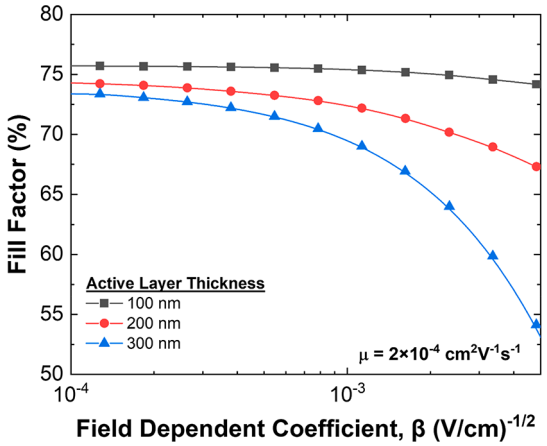

Figure 1. Simulated device FF at different field-dependent coefficients (β) and active layer thicknesses (100, 200, and 300 nm).

https://doi.org/10.1021/acsami.2c11265
ACS Appl. Mater. Interfaces 2022, 14, 47961−47970

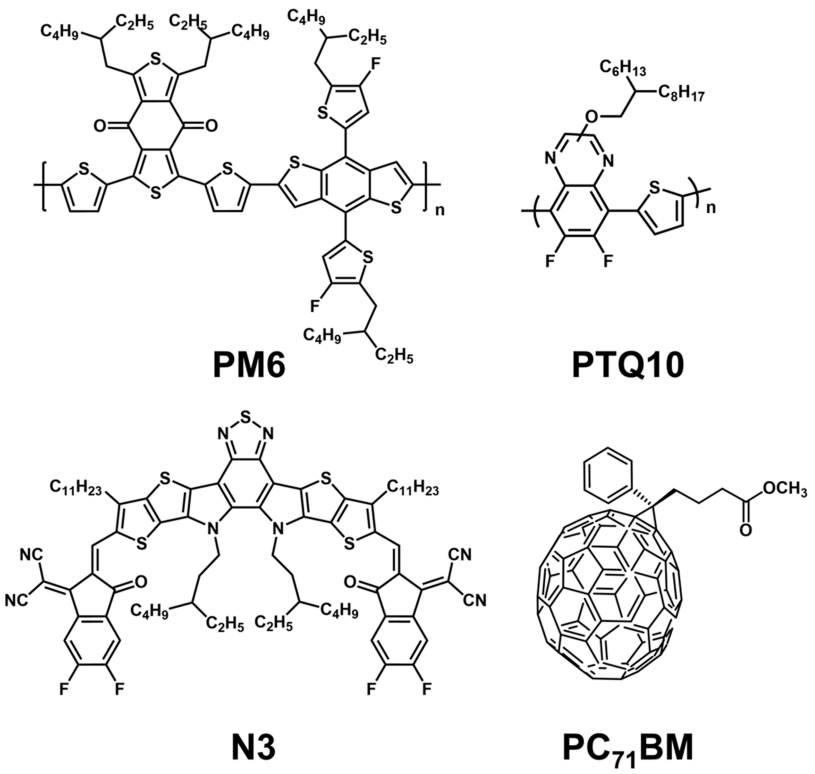

Figure 2. Chemical structures of active layer materials used in this study.

larger than 10^{-3} $(V/cm)^{-1/2}$. For example, when $\beta = 5 \times 10^{-3}$ $(V/cm)^{-1/2}$, the FF drops from 74% to 54% as the active layer thickness increases from 100 nm to 300 nm. Only for β smaller than this value, the device's FF can remain above 70% even with a 300 nm thick active layer. In the following sections, we will validate the importance of mobility field-dependent coefficient with device data and present the details.

2.2. Field-Dependent Charge Carrier Mobilities. The chemical structures of PM6, PTQ10, N3, and $PC_{71}BM$ are shown in Figure 2. Both PM6:N3:$PC_{71}BM$ and PTQ10:N3:$PC_{71}BM$ blends have similar absorption spectral characteristics between 400 nm and 950 nm (Supporting Information Figure S1). The donor polymers PM6 and PTQ10 are chosen because they have very similar absorption spectra along with similar device performance in thin devices.[30,32] For acceptors, instead of the commonly used NFA Y6, we used N3 because it exhibits good solubility, electronic properties, and morphological properties.[32] $PC_{71}BM$ was added into the BHJ blends to increase the molecular packing and improve the electron transport.[33] Single-carrier devices are devices that transport either only electrons (electron-only) or only holes (holes-only) and hence can be used to characterize the electron and hole transport, respectively. Electron-only devices having a structure of ITO/ZnO/active layer/PDINO/Al and hole-only devices with structure ITO/PEDOT:PSS/active layer/MoO_x/Ag were fabricated according to the details provided in the Experimental Section. The current−voltage characteristics of those devices can be found in Figure S3a. To understand the thickness-dependent FF behavior, we first extracted the charge carrier parameters in the BHJ films using a modified Mott−Gurney equation:

$$J_{SCL}d = \frac{9}{8}\varepsilon_0\varepsilon_r\mu_0 \exp(0.89\beta\sqrt{F})F^2 \quad (2)$$

where J_{SCL} is the space−charge limited current density, d is the thickness of the active layer, ε_0 is the permittivity of vacuum, and ε_r is the relative permittivity of the polymer.[34,35] The $J-V$ characteristics of electron-only and hole-only devices of PM6 and PTQ10 blends are shown in Figure S3a. The extracted μ_0 and β values from the hole-only and electron-only devices are summarized in Table 1. We note that the PTQ10 blend has a smaller value of β for both holes and electrons. The extracted μ_0 and β values were used to reconstruct the field-dependent mobility $\mu(F)$ as shown in Figure S3b.

Table 1. Extracted Zero-Field Mobility (μ_0) and Field-Dependent Coefficient (β) from SCLC Measurements[a]

Active Layer Blend	Device Structure	μ_0(cm^2 V^{-1} s^{-1})	β ($(V/cm)^{-1/2}$)
PM6	hole-only	1.34×10^{-4}	4.48×10^{-3}
	electron-only	3.34×10^{-4}	2.25×10^{-3}
PTQ10	hole-only	3.89×10^{-4}	1.20×10^{-3}
	electron-only	3.67×10^{-4}	4.84×10^{-4}

[a]The SCLC $J-V$ characteristics can be found in Figure S3.

In a thin-film PV cell, the operating electric field ranges between the short-circuit condition ($F = V_{OC}/d$) and the open-circuit condition ($F = 0$). Because the PM6 blend and PTQ10 blend have similar V_{OC}, we estimate the square root electric field strength to be 290 $(V/cm)^{1/2}$ and 170 $(V/cm)^{1/2}$ in the 100 nm and 300 nm thick active layers, respectively. To further understand charge extraction in both devices, the field-dependent electron mobility and hole mobility with different active layers are then extrapolated as shown in Figure 3. It can be clearly seen that, in the PTQ10 blend, the electron and hole mobilities have a lower field dependence throughout the entire electric field strength relevant to the thick cell. On the other hand, the PM6 blend shows a higher field dependence,

https://doi.org/10.1021/acsami.2c11265
ACS Appl. Mater. Interfaces 2022, 14, 47961−47970

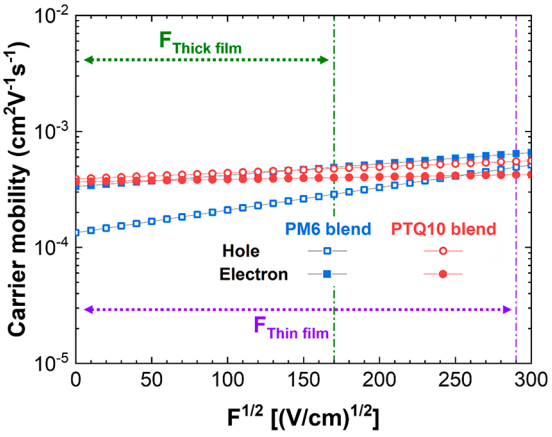

Figure 3. Extrapolated electron mobilities (solid symbols) and hole mobilities (open symbols) at different field strengths for PM6 (blue) and PTQ10 (red) blends. The brown and green vertical dashed lines represent the maximum internal electric field strength inside the thin-film and thick-film OSCs, respectively.

especially for hole transport. To verify the field-dependent transport characteristic extracted from SCLC, we also performed admittance spectroscopy (AS) on electron-only devices. In AS, the device is placed under a forward DC voltage bias with a small AC perturbation and the modulation frequency-dependent capacitances are obtained. From a plot of negative differential susceptance ($-\Delta B$) vs frequency (f), a maximum in the $-\Delta B$ plot defines the corresponding frequency (f_r) which can be used to compute the carrier mobility by the relation $\mu = \frac{d^2}{(0.56 f_r^{-1}) V_{DC}}$, where d is the thickness of the active layer and V_{DC} is the direct current biased voltage.[36−39] By repeating the frequency-dependent capacitance measurement at different V_{DC}s, the field dependence of mobility can be extracted. As shown in Figure S4, the β values for the PM6 blend and the PTQ10 blends were 5.5×10^{-3} $(V/cm)^{-1/2}$ and 4.2×10^{-3} $(V/cm)^{-1/2}$, respectively, which are in good agreement with our findings using modified Mott−Gurney eq 2. To see the effects of the carrier mobility on the device FF, a simulation was done on the FF as a function of the β value of a cell with an active layer thickness of 300 nm for different mobility values, and the results are shown in Figure S5. It is clear that a mobility value of 8×10^{-4} $cm^2/(V\ s)$ and $\beta < 1 \times 10^{-4}$ $(V/cm)^{-0.5}$ are needed to maintain a high FF for thick-film BHJ OSCs.

2.3. Thickness-Dependent Solar Cell Performance. Optical interference effects can influence the optimization of active layer thickness. Interference between the incident light and back-reflected light from the bottom electrode can prevent the percentage of light absorbed by the active layer from increasing monotonically with thickness, giving rise to several local maxima in the J_{SC} vs active layer thickness plot.[40] Using the transfer-matrix method, we simulated the spectral light utilization of OSCs for different active layer thicknesses (Figure 4a). The transfer-matrix method uses Maxwell's equations and electric-field-continuity conditions across device boundaries and interfaces to calculate the electric field within the device from a simple matrix operation.[41] Considering the spectral absorbance for film thicknesses of ∼100 nm and ∼300 nm, there are two absorption local maxima in the 100 nm thick film with a weak absorption at 650 nm, while there is a broad optical absorption band from 450 nm to 900 nm for the 300

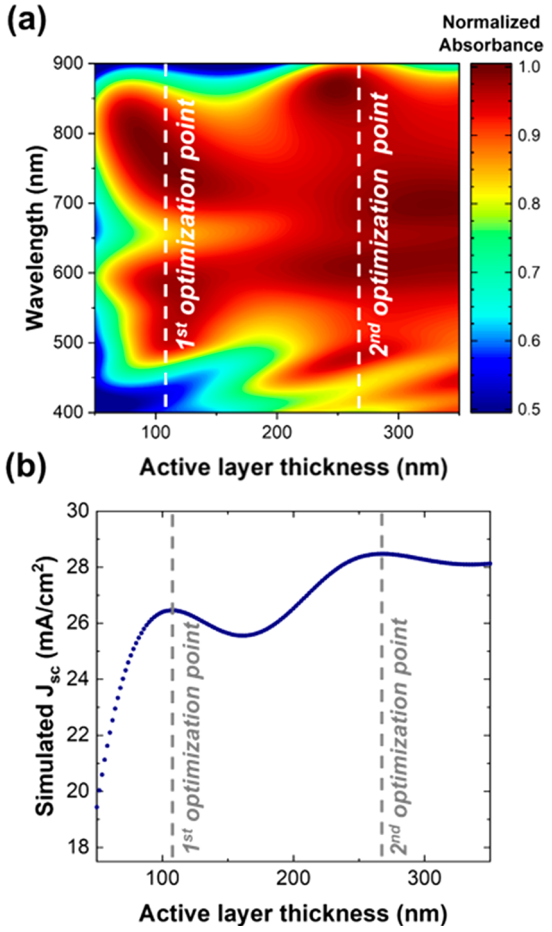

Figure 4. (a) Simulated optical absorbance at different wavelengths and active layer thicknesses. (b) Calculated OSC J_{SC} at different active-layer thicknesses, assuming the open-circuit voltage and FF are kept constant.

nm thick film. By integrating over the absorption spectrum of the active layer, the 300 nm thick active layer yields a higher short-circuit current density (J_{SC}), as shown in Figure 4b and should give a higher PCE than a 100 nm thick cell.

To fabricate OSCs used in this work, we used the inverted structure ITO/ZnO/active layer/MoO_x/Ag. Detailed device fabrication procedures are described in the Experimental Section. The key photovoltaic parameters under AM1.5G illumination (PCE, FF, and J_{SC}) of all OSCs are shown in Figure 5. In terms of PCE, both BHJ blends show a local maximum at ∼100 nm thick active layer, where the corresponding PCEs of PM6 and PTQ10 are 16.2% and 16.0%, respectively. Both thin-film devices yield a FF larger than 75%. The J_{SC} for both ternary blends vary with the active layer thickness due to optical interference, reaching a local minimum at a thickness of about 150 nm and a local maximum at about 300 nm. For the PM6 blend, as the active layer thickness increases to 300 nm, there is a substantial drop in the FF to 50%, resulting in a lower PCE of 10.4%. On the other hand, the trend is very different in the PTQ10 blend. Similar to the PM6 blend, there is also a local maximum in J_{SC}. There is only a small drop in FF from 77% to 74% when the active layer thickness increases from 100 nm to 300 nm, while J_{SC} increases slightly from 23.5 mA/cm^2 to 26.8 mA/cm^2, and the resulting 300 nm thick PTQ10:N3:$PC_{71}BM$ blend OSC yields a high PCE of 16.8%, which is among the highest for thick-film OPVs.

https://doi.org/10.1021/acsami.2c11265
ACS Appl. Mater. Interfaces 2022, 14, 47961−47970

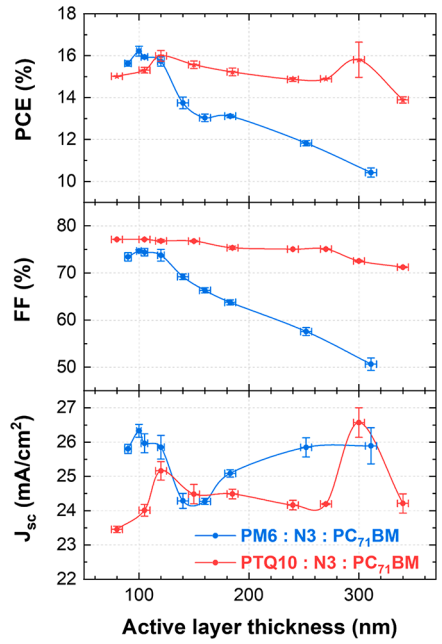

Figure 5. Key photovoltaic parameters of PM6:N3:$PC_{71}BM$ and PTQ10:N3:$PC_{71}BM$ OSC devices at different active layer thicknesses.

The current density−voltage (J−V) characteristic and the performance parameters of the 300 nm thick PTQ10 blend OSC are also shown in Figure 6. In our previous study, we

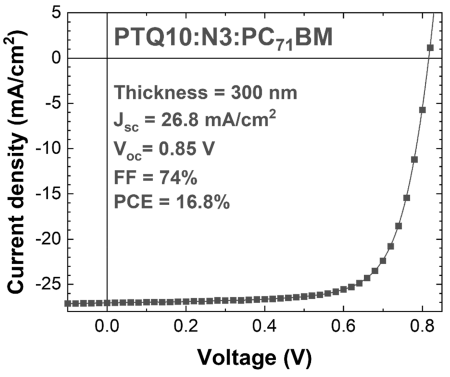

Figure 6. J−V characteristics of the best thick-film PTQ10:N3:$PC_{71}BM$ OSC under AM1.5G solar spectrum.

demonstrated that FF-optimized donor−acceptor ratio possesses better balanced field-dependent hole-to-electron ratios due to the weak field-dependent electron mobilities.[42] Putting the extracted transport parameters back into the simulation in Figure 1, we obtained a good agreement between the experimental and simulated FF for both materials with different active layer thicknesses.

2.4. Charge Recombination and Trap Analysis. It is been well-established that the bimolecular recombination is the main factor for the reduced charge transport and the FF drop, while the first order recombination or trap-assisted recombination is usually well-suppressed in many high-efficiency OPV systems.[7,43] To investigate the charge recombination behavior in different BHJ blends and correlate them with their thickness-dependent FF values, the J−V characteristics of OSCs were measured under different light intensities, ranging from 1 mW/cm^2 to 100 mW/cm^2 (Figure S6). J_{SC} and V_{OC} are plotted against light intensity in Figure 7. The J_{SC} dependence on light intensity (P_{light}) can be expressed as $J_{SC} \propto (P_{light})^{\alpha}$.[44,45] The bimolecular recombination is considered weak if α is close to unity and strong otherwise.[45] The fitted α values of all samples are within 0.940−0.950, suggesting bimolecular recombination is negligible in all devices with different active layer thicknesses, and there is no significant difference between the PM6 blend and PTQ10 blend. To evaluate trap-assisted recombination, the V_{OC} dependence on light intensity is expressed as

$$V_{OC} \propto n\left(\frac{kT}{q}\right)\ln(P_{light}) \tag{3}$$

where n is the ideality factor, k is the Boltzmann constant, T is temperature in kelvin, and q is the charge of the electron. n can be obtained from the slope of the semilogarithmic curve V_{OC} vs $\ln(P_{light})$. When n = 1, then OSC can be described using the drift−diffusion model, where the quasi-Fermi levels are aligned across the OSC without any recombination due to trap states. In the case of n = 2, the trap-assisted recombination becomes dominant.[46,47] The fitted n values of the PM6 blend thin film, PTQ10 blend thin film, and PTQ10 blend thick film are all within 1.1. The higher n = 1.22 ± 0.02 in the thick-film PM6 blend indicates a slightly higher trap-assisted recombination, and it is consistent with a lower FF value in a PM6 blend thick-film OSC, which is evident in Figure S6b in the region between the short-circuit and the maximum power points.[47] This trap-assisted recombination has been identified as a factor affecting FF.[47,48]

We also investigated the energetic disorder in the active layers using photothermal deflection spectroscopy (PDS).[49−53] PDS is commonly used to characterize the degree of energetic disorder in disordered materials and organic semiconductors by analyzing the absorption tail with a characteristic Urbach energy (E_u) below the band gap.[54,55] A smaller E_u represents a smaller energetic disorder. As shown in Figure S7, the fitted values of E_u of PM6:N3:$PC_{71}BM$ and PTQ10:N3:$PC_{71}BM$ blends are 26 ± 0.4 meV and 28 ± 0.5 meV, respectively, suggesting that the PTQ10 blend has a lower energetic disorder than the PM6 blend.[53,56] These results are consistent with the results from Zhang et al. and Ng et al. showing that a low E_u value in the active layer results in a higher charge carrier mobility and device FF.[57,58] The results from the PDS measurements are also consistent with the findings in the field-dependent mobility measurements and recombination from the light-dependent analysis. A higher E_u value stipulates the existence of deeper traps that can act as charge recombination centers, impacting the charge carrier mobility. This effect is more pronounced in the low electric field regime, leading to a drop in FF with increasing active layer thickness.

2.5. Material Vertical Distribution and Molecular Packing. Secondary-ion mass spectroscopy (SIMS) was further used to characterize the vertical composition gradients with respect to different active layer thicknesses.[59,60] Since there are no unique chemical elements among PM6, PTQ10, N3, and $PC_{71}BM$, we replaced $PC_{71}BM$ with deuterated $PC_{61}BM$ (d-$PC_{61}BM$) and traced the deuterium signal ($^2H^-$). The full SIMS profiles can be found in Figure S8, showing the scanned area from the top Ag anode to the bottom ITO cathode. The SIMS fragment profiles clearly reflect the thicknesses of interlayers and active layers. Fullerene is known to be partially miscible with PM6 and PTQ10.[61,62] It

https://doi.org/10.1021/acsami.2c11265
ACS Appl. Mater. Interfaces 2022, 14, 47961−47970

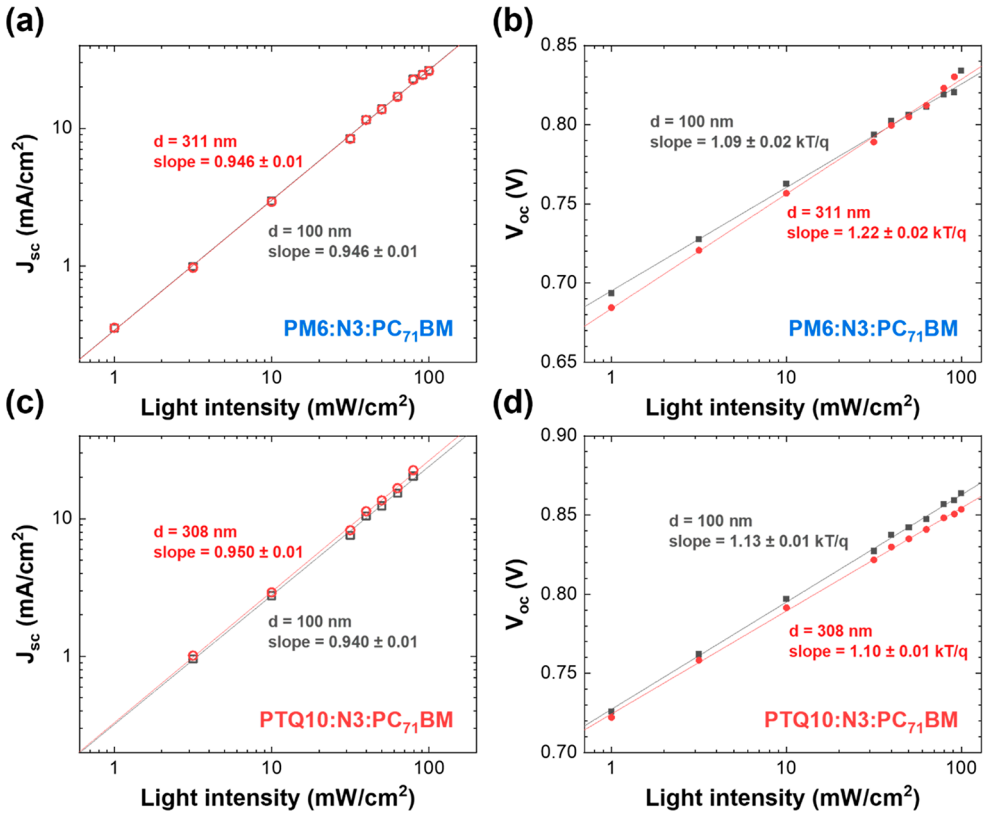

Figure 7. Dependence of J_{SC} and V_{OC} on light intensity for (a, b) PM6:N3:$PC_{71}BM$ and (c, d) PTQ10:N3:$PC_{71}BM$ films.

is thus reasonable to assume that $^{2}H^{-}$ tracks the vertical distribution of the donor polymer at the concentration levels of d-$PC_{61}BM$ used. Generally, SIMS indicates donor and PCBM enrichment near the anode in PM6-based devices, whereas thin PTQ10-based devices are acceptor-rich near the anode with a negligible gradient for the thicker devices. Considering the relatively small amount of fullerene content in the active layer blends, the fullerene will first dock with the donor polymer before self-aggregating. On the basis of this assumption, we use the $^{2}H^{-}$ signal to track the vertical distribution of the donor polymer. We calculated the slope of $^{2}H^{-}$ to quantify the donor polymer distribution to make a better comparison (Figure S9). Although vertical gradients have been previously associated with differences in performance, the canonical interpretation that donor enrichment near the anode is favorable would suggest that the PM6-based devices should be superior.[61] This is clearly not the case, and the favorable impact of the gradient had to be overcome by a stronger factor.

Next, we simulated the charge generation profile throughout the OSC with different active layer thicknesses using the transfer-matrix method. The results are shown in Figure 8. While charge generation in the active layer is close to the ZnO interlayer in both thin and thick films, we noticed an additional charge generation at a position close to the top silver electrode in the thick active layer. This observation can be interpreted in terms of the relative motion of the holes in the films with respect to the electrons. In thin layers, holes traverse only a slightly longer distance to the anode compared to electrons traveling to the cathode, while, in thick films, holes need to travel a much longer distance to reach the anode. An unbalanced electron and hole mobility with increasing carrier travel distance exaggerates the space−charge effect and hence reduces the FF in thick-film solar cells.

A schematic diagram describing the effects of the donor polymer vertical distribution on thick-film OSC performance is depicted in Figure S10. First, as shown in the charge generation profile simulation, most excitons are generated in the active layer close to the cathode. Once excitons are separated into electron−hole pairs, holes are transported through the donor polymer and electrons are transported through the acceptor molecules. In the PM6:N3:$PC_{71}BM$ blend, since the region near the cathode is acceptor-rich, the hole transport pathway is less percolated near the ZnO interface. The dead-ends of the hole transport pathways are hindered by the presence of traps, increasing charge recombination as reflected from the light-intensity-dependent and PDS measurements, and a weaker electric field in the thick device leads to an imbalanced field-dependent hole−electron mobility. In contrast, evenly vertically distributed PTQ10 donor polymers provide a well-connected hole transport pathway from the exciton generation position to the anode, resulting in a higher FF in the thick-film PTQ10:N3:$PC_{71}BM$ OSC.

3. CONCLUSION

We have successfully demonstrated the mobility field-dependent coefficient is a critical parameter determining the field factor loss in thick-film OSCs. Using device simulations based on a drift−diffusion model, we show that a mobility field-dependent coefficient β smaller than 10^{-3} $(V/cm)^{-1/2}$ is required to maintain a good FF (>70%) in thick-film devices. Using PTQ10:N3:$PC_{71}BM$ and PM6:N3:$PC_{71}BM$ blends as illustrations, we show that the experimental results for FF and corresponding β value are in good agreement with the simulation results. Specifically, we show that a high PCE of

https://doi.org/10.1021/acsami.2c11265
ACS Appl. Mater. Interfaces 2022, 14, 47961−47970

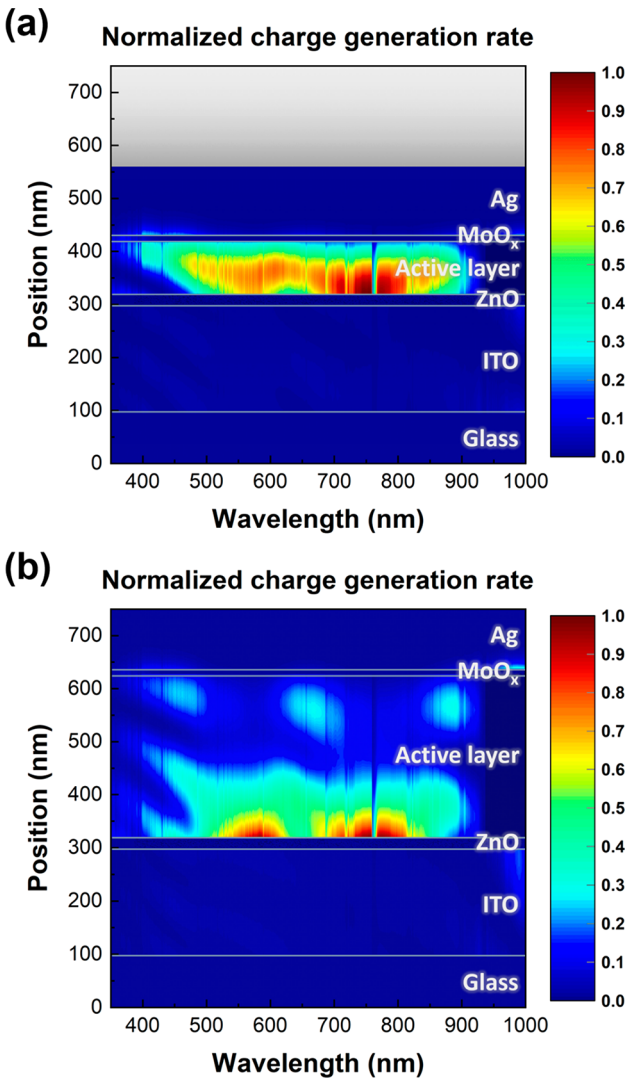

Figure 8. Simulated relative charge generation rate distribution profile at active layer thicknesses of (a) 100 and (b) 300 nm.

16.8% is realized for thick-film BHJ PTQ10 cells. Such a high FF in the thick PTQ10 blend film is also consistent with the observation of lower charge recombination from light-intensity-dependent measurements, a smaller Urbach tail from photothermal deflection spectroscopy, and a more uniform vertical phase distribution from secondary-ion mass spectrometry. Our results provide a clear path forward for developing thick-film OPV devices compatible with manufacturing processes in the future.

4. EXPERIMENTAL SECTION

4.1. Materials. Poly[(2,6-(4,8-bis(5-(2-ethylhexyl-3-fluoro)-thiophen-2-yl)-benzo[1,2-*b*:4,5-*b*′]dithiophene))-*alt*-(5,5-(1′,3′-di-2-thienyl-5′,7′-bis(2-ethylhexyl)benzo[1′,2′-*c*:4′,5′-*c*′]dithiophene-4,8-dione)] (PM6) and 2,2′-((2*Z*,2′*Z*)-((12,13-bis(3-ethylheptyl)-3,9-diundecyl-12,13-dihydro[1,2,5]thiadiazolo[3,4-*e*]thieno[2″,3″:4′,5′]-thieno[2′,3′:4,5]pyrrolo[3,2-g]thieno[2′,3′:4,5]thieno[3,2-*b*]indole-2,10-diyl)bis(methanylylidene))bis(5,6-difluoro-3-oxo-2,3-dihydro-1*H*-indene-2,1-diylidene))dimalononitrile (N3) were purchased from eFlexPV. [6,6]-Phenyl-C71-butyric acid methyl ester ($PC_{71}BM$) was purchase from nano-C. Poly[(thiophene)-*alt*-(6,7-difluoro-2-(2-hexyldecyloxy)quinoxaline)] (PTQ10) was synthesized as reported previously. All materials were used as received.

4.2. Organic Solar Cell Fabrication. The device structure of a single-OPV device was ITO/ZnO/active layer/MoO_x/Ag. An ITO patterned glass substrate was cleaned by acetone and isopropanol in an ultrasonic bath followed by UV−ozone treatment. ZnO sol−gel was then spin-coated at 4000 rpm onto the ITO substrate and thermally annealed at 150 °C for 30 min. The donor polymer:N3:$PC_{71}BM$ is blended in a weight ratio of 1:1.2:0.2. The active layer blends were than dissolved in chloroform with a total concentration of 22 mg/mL. The solution was then spin-coated on ZnO covered substrates and annealed at 110 °C for 5 min. Finally, 10 nm of MoO_x and 120 nm of Ag were thermally evaporated.

4.3. Single-Carrier Device Fabrication. Electron-only devices had a structure of ITO/ZnO/active layer/PDINO/Al, and hole-only devices had a structure of ITO/PEDOT:PSS/active layer/MoO_x/Ag. In electron-only devices, *N*,*N*-dimethylammonium *N*-oxide)propyl perylene diimide (PDINO), which was dissolved in methanol with 2 mg/mL concentration, was spin-coated at 5000 rpm on top of the active layer. In hole-only devices, PEDOT:PSS—poly(3,4-ethylenedioxythiophene) polystyrenesulfonate—was spin-coated at 7000 rpm for 60 s and then thermally annealed at 150 °C for 10 min. The other layers followed the same procedures as normal devices.

4.4. Admittance Spectroscopy (AS). The single-carrier device was put in an Oxford cryostat with a pressure of less than 20 mTorr for measurement. The admittances of all devices were measured by an impedance analyzer (Hioki E. E. Corp., Model 3532-50 LCR HiTESTER). An alternating current modulation of an amplitude of 50 mV was superimposed on a direct current bias voltage to obtain the AS signal.

4.5. Photothermal Deflection Spectroscopy (PDS). PDS measurements were carried out with a standard setup consisting of a 1 kW Xe arc lamp and a 1/4 m grating monochromator (Oriel) as the tunable light source. The pump beam was modulated at 13 Hz by a mechanical chopper before irradiating on the sample. Perfluorohexane was used as the deflection fluid. A Uniphase HeNe laser was directed parallel to the polymer sample surface as the probe laser. A quadrant cell (United Detector Technology) was used as the position sensor for monitoring the photothermal deflection signal of the probe beam. The output of the detector was fed into a lock-in amplifier (Stanford Research, Model SR830) for phase-sensitive measurements. All PDS spectra were normalized to the incident power of the pump beam.

4.6. Time-of-Flight Secondary-Ion Mass Spectrometry (SIMS). The SIMS characterizations were carried out in a time-of-flight secondary-ion mass spectrometer (TOF-SIMS) (ION TOF V, Inc. Chestnut Ridge, NY, USA) at NCSU. Dual-beam dynamic SIMS mode was used to provide high depth resolution and chemical resolution simultaneously, where Bi^+ was employed as the primary ion and Cs^+ was employed as the sputtering source. $^2H^-$ molecular component was selected to monitor the d-$PC_{61}BM$ depth profile. The analysis chamber pressure is maintained below 5.0×10^{-9} mbar to avoid contamination of the surfaces to be analyzed.

■ ASSOCIATED CONTENT

Supporting Information

The Supporting Information is available free of charge at https://pubs.acs.org/doi/10.1021/acsami.2c11265.

active layer materials' normalized absorption spectra; *J*−*V* characteristics; electric-field-dependent electron mobilities extracted from admittance spectroscopy, simulated device FFs; photothermal deflection spectroscopy results; SIMS depth profiles; charge transport schematic diagram; donor polymers' vertical distribution(PDF)

■ AUTHOR INFORMATION

Corresponding Authors

Carr Hoi Yi Ho − *Department of Materials Science and Engineering, and Organic and Carbon Electronics*

https://doi.org/10.1021/acsami.2c11265
ACS Appl. Mater. Interfaces 2022, 14, 47961−47970

Laboratories (ORaCEL), North Carolina State University Raleigh, Raleigh, North Carolina 27695, United States; Email: hohoiyicarr@gmail.com

Franky So − *Department of Materials Science and Engineering, and Organic and Carbon Electronics Laboratories (ORaCEL), North Carolina State University Raleigh, Raleigh, North Carolina 27695, United States*; orcid.org/0000-0002-8310-677X; Email: fso@ncsu.edu

Authors

Yusen Pei − *Department of Materials Science and Engineering, and Organic and Carbon Electronics Laboratories (ORaCEL), North Carolina State University Raleigh, Raleigh, North Carolina 27695, United States*

Yunpeng Qin − *Department of Physics, and Organic and Carbon Electronics Laboratories (ORaCEL), North Carolina State University Raleigh, Raleigh, North Carolina 27695, United States*

Chujun Zhang − *Department of Physics and Institute of Advanced Materials, Hong Kong Baptist University, Hong Kong, People's Republic of China*

Zhengxing Peng − *Department of Physics, and Organic and Carbon Electronics Laboratories (ORaCEL), North Carolina State University Raleigh, Raleigh, North Carolina 27695, United States*; orcid.org/0000-0002-7871-1158

Indunil Angunawela − *Department of Physics, and Organic and Carbon Electronics Laboratories (ORaCEL), North Carolina State University Raleigh, Raleigh, North Carolina 27695, United States*

Austin L. Jones − *School of Chemistry and Biochemistry School of Materials Science and Engineering Center for Organic Photonics and Electronics, Georgia Tech Polymer Network, Georgia Institute of Technology, Atlanta, Georgia 30332, United States*

Hang Yin − *Department of Physics and Institute of Advanced Materials, Hong Kong Baptist University, Hong Kong, People's Republic of China*

Hamna F. Iqbal − *Department of Materials Science and Engineering, and Organic and Carbon Electronics Laboratories (ORaCEL), North Carolina State University Raleigh, Raleigh, North Carolina 27695, United States*

John R. Reynolds − *School of Chemistry and Biochemistry School of Materials Science and Engineering Center for Organic Photonics and Electronics, Georgia Tech Polymer Network, Georgia Institute of Technology, Atlanta, Georgia 30332, United States*; orcid.org/0000-0002-7417-4869

Kenan Gundogdu − *Department of Physics, and Organic and Carbon Electronics Laboratories (ORaCEL), North Carolina State University Raleigh, Raleigh, North Carolina 27695, United States*; orcid.org/0000-0001-7149-5766

Harald Ade − *Department of Physics, and Organic and Carbon Electronics Laboratories (ORaCEL), North Carolina State University Raleigh, Raleigh, North Carolina 27695, United States*

Shu Kong So − *Department of Physics and Institute of Advanced Materials, Hong Kong Baptist University, Hong Kong, People's Republic of China*

Complete contact information is available at: https://pubs.acs.org/10.1021/acsami.2c11265

Notes

The authors declare no competing financial interest.

ACKNOWLEDGMENTS

This work was supported by NextGen Nano Ltd.; Office of Naval Research Grants N00014-17-1-2242, N00014-17-1-2243, and N000142012155; National Science Foundation Award CBET-1639429; and the UNC General Administration Research Opportunity Initiative grant. X-ray data were acquired at beamlines 11.0.1.2 and 7.3.3 at the Advanced Light Source, which is supported by the Director, Office of Science, Office of Basic Energy Sciences, of the U.S. Department of Energy under Contract No. DE-AC02-05CH11231.

REFERENCES

(1) Kang, H.; Kim, G.; Kim, J.; Kwon, S.; Kim, H.; Lee, K. Bulk-Heterojunction Organic Solar Cells: Five Core Technologies for Their Commercialization. *Adv. Mater.* **2016**, *28* (36), 7821−7861.

(2) Li, C.; Zhou, J.; Song, J.; Xu, J.; Zhang, H.; Zhang, X.; Guo, J.; Zhu, L.; Wei, D.; Han, G.; Min, J.; Zhang, Y.; Xie, Z.; Yi, Y.; Yan, H.; Gao, F.; Liu, F.; Sun, Y. Non-Fullerene Acceptors with Branched Side Chains and Improved Molecular Packing to Exceed 18% Efficiency in Organic Solar Cells. *Nat. Energy* **2021**, *6* (6), 605−613.

(3) Liu, F.; Zhou, L.; Liu, W.; Zhou, Z.; Yue, Q.; Zheng, W.; Sun, R.; Liu, W.; Xu, S.; Fan, H.; Feng, L.; Yi, Y.; Zhang, W.; Zhu, X. Organic Solar Cells with 18% Efficiency Enabled by an Alloy Acceptor: A Two-in-One Strategy. *Adv. Mater.* **2021**, *33* (27), 2100830.

(4) Liu, Q.; Jiang, Y.; Jin, K.; Qin, J.; Xu, J.; Li, W.; Xiong, J.; Liu, J.; Xiao, Z.; Sun, K.; Yang, S.; Zhang, X.; Ding, L. 18% Efficiency Organic Solar Cells. *Sci. Bull.* **2020**, *65* (4), 272−275.

(5) Gao, J.; Wang, J.; Xu, C.; Hu, Z.; Ma, X.; Zhang, X.; Niu, L.; Zhang, J.; Zhang, F. A Critical Review on Efficient Thick-Film Organic Solar Cells. *Sol. RRL* **2020**, *4* (11), 2000364.

(6) Zhang, D.; Fan, B.; Ying, L.; Li, N.; Brabec, C. J.; Huang, F.; Cao, Y. Recent Progress in Thick-film Organic Photovoltaic Devices: Materials, Devices, and Processing. *SusMat* **2021**, *1* (1), 4−23.

(7) Bartesaghi, D.; Pérez, I. D. C.; Kniepert, J.; Roland, S.; Turbiez, M.; Neher, D.; Koster, L. J. A. Competition between Recombination and Extraction of Free Charges Determines the Fill Factor of Organic Solar Cells. *Nat. Commun.* **2015**, *6* (1), 7083.

(8) Jao, M.-H.; Liao, H.-C.; Su, W.-F. Achieving a High Fill Factor for Organic Solar Cells. *J. Mater. Chem. A* **2016**, *4* (16), 5784−5801.

(9) Qi, B.; Wang, J. Fill Factor in Organic Solar Cells. *Phys. Chem. Chem. Phys.* **2013**, *15* (23), 8972.

(10) Ma, L.; Xu, Y.; Zu, Y.; Liao, Q.; Xu, B.; An, C.; Zhang, S.; Hou, J. A Ternary Organic Solar Cell with 300 Nm Thick Active Layer Shows over 14% Efficiency. *Sci. China Chem.* **2020**, *63* (1), 21−27.

(11) Zhan, L.; Li, S.; Lau, T.-K.; Cui, Y.; Lu, X.; Shi, M.; Li, C.-Z.; Li, H.; Hou, J.; Chen, H. Over 17% Efficiency Ternary Organic Solar Cells Enabled by Two Non-Fullerene Acceptors Working in an Alloy-like Model. *Energy Environ. Sci.* **2020**, *13* (2), 635−645.

(12) Gao, J.; Gao, W.; Ma, X.; Wang, J.; Wang, X.; Xu, C.; Zhang, X.; Zhang, J.; Yang, C.; Jen, A. K.-Y.; Zhang, F. Over 16% Efficiency of Thick-Film Organic Photovoltaics with Symmetric and Asymmetric Non-Fullerene Materials as Alloyed Acceptor. *Sol. RRL* **2021**, *5* (8), 2100365.

(13) Shieh, J.-T.; Liu, C.-H.; Meng, H.-F.; Tseng, S.-R.; Chao, Y.-C.; Horng, S.-F. The Effect of Carrier Mobility in Organic Solar Cells. *J. Appl. Phys.* **2010**, *107* (8), 084503.

(14) Hosseini, S. M.; Tokmoldin, N.; Lee, Y. W.; Zou, Y.; Woo, H. Y.; Neher, D.; Shoaee, S. Putting Order into PM6:Y6 Solar Cells to Reduce the Langevin Recombination in 400 Nm Thick Junction. *Sol. RRL* **2020**, *4* (11), 2000498.

(15) Shoaee, S.; Armin, A.; Stolterfoht, M.; Hosseini, S. M.; Kurpiers, J.; Neher, D. Decoding Charge Recombination through Charge Generation in Organic Solar Cells. *Sol. RRL* **2019**, *3* (11), 1900184.

(16) Armin, A.; Subbiah, J.; Stolterfoht, M.; Shoaee, S.; Xiao, Z.; Lu, S.; Jones, D. J.; Meredith, P. Reduced Recombination in High

Efficiency Molecular Nematic Liquid Crystalline: Fullerene Solar Cells. *Adv. Energy Mater.* **2016**, *6* (22), 1600939.
(17) Stolterfoht, M.; Shoaee, S.; Armin, A.; Jin, H.; Kassal, I.; Jiang, W.; Burn, P.; Meredith, P. Electric Field and Mobility Dependent First-Order Recombination Losses in Organic Solar Cells. *Adv. Energy Mater.* **2017**, *7* (4), 1601379.
(18) Chang, Y.; Zhu, X.; Lu, K.; Wei, Z. Progress and Prospects of Thick-Film Organic Solar Cells. *J. Mater. Chem. A* **2021**, *9* (6), 3125−3150.
(19) Blakesley, J. C.; Castro, F. A.; Kylberg, W.; Dibb, G. F. A.; Arantes, C.; Valaski, R.; Cremona, M.; Kim, J. S.; Kim, J.-S. Towards Reliable Charge-Mobility Benchmark Measurements for Organic Semiconductors. *Org. Electron.* **2014**, *15* (6), 1263−1272.
(20) Haneef, H. F.; Zeidell, A. M.; Jurchescu, O. D. Charge Carrier Traps in Organic Semiconductors: A Review on the Underlying Physics and Impact on Electronic Devices. *J. Mater. Chem. C* **2020**, *8* (3), 759−787.
(21) Movaghar, B.; Jones, L. O.; Ratner, M. A.; Schatz, G. C.; Kohlstedt, K. L. Are Transport Models Able To Predict Charge Carrier Mobilities in Organic Semiconductors? *J. Phys. Chem. C* **2019**, *123* (49), 29499−29512.
(22) Lu, L. Refinement on the Theories of Measurement for Trap Density from Space-charge-limited Current. *J. Appl. Phys.* **1993**, *73* (1), 261−264.
(23) Nešpůrek, S.; Zmeškal, O.; Sworakowski, J. Space-Charge-Limited Currents in Organic Films: Some Open Problems. *Thin Solid Films* **2008**, *516* (24), 8949−8962.
(24) Tse, S. C.; Tsang, S. W.; So, S. K. Polymeric Conducting Anode for Small Organic Transporting Molecules in Dark Injection Experiments. *J. Appl. Phys.* **2006**, *100* (6), 063708.
(25) Blom, P. W. M. Polymer Electronics: To Be or Not to Be? *Adv. Mater. Technol.* **2020**, *5* (6), 2000144.
(26) Li, L.; Van Winckel, S.; Genoe, J.; Heremans, P. Electric Field-Dependent Charge Transport in Organic Semiconductors. *Appl. Phys. Lett.* **2009**, *95* (15), 153301.
(27) Shirota, Y.; Kageyama, H. Charge Carrier Transporting Molecular Materials and Their Applications in Devices. *Chem. Rev.* **2007**, *107* (4), 953−1010.
(28) Yin, H.; Ma, L.-K.; Yan, J.; Zhang, Z.; Cheung, A. M. H.; Zhang, J.; Yan, H.; So, S. K. Thick-Film Low Driving-Force Indoor Light Harvesters. *Sol. RRL* **2020**, *4* (10), 2000291.
(29) Liguori, R.; Rubino, A. Admittance Spectroscopy and Material Modeling for Organic Electronic Applications. *Mater. Today Proc.* **2021**, *44*, 2033−2037.
(30) Sun, C.; Pan, F.; Bin, H.; Zhang, J.; Xue, L.; Qiu, B.; Wei, Z.; Zhang, Z.-G.; Li, Y. A Low Cost and High Performance Polymer Donor Material for Polymer Solar Cells. *Nat. Commun.* **2018**, *9* (1), 743.
(31) Yao, N.; Wang, J.; Chen, Z.; Bian, Q.; Xia, Y.; Zhang, R.; Zhang, J.; Qin, L.; Zhu, H.; Zhang, Y.; Zhang, F. Efficient Charge Transport Enables High Efficiency in Dilute Donor Organic Solar Cells. *J. Phys. Chem. Lett.* **2021**, *12* (20), 5039−5044.
(32) Jiang, K.; Wei, Q.; Lai, J. Y. L.; Peng, Z.; Kim, H. K.; Yuan, J.; Ye, L.; Ade, H.; Zou, Y.; Yan, H. Alkyl Chain Tuning of Small Molecule Acceptors for Efficient Organic Solar Cells. *Joule* **2019**, *3* (12), 3020−3033.
(33) Arunagiri, L.; Peng, Z.; Zou, X.; Yu, H.; Zhang, G.; Wang, Z.; Lin Lai, J. Y.; Zhang, J.; Zheng, Y.; Cui, C.; Huang, F.; Zou, Y.; Wong, K. S.; Chow, P. C. Y.; Ade, H.; Yan, H. Selective Hole and Electron Transport in Efficient Quaternary Blend Organic Solar Cells. *Joule* **2020**, *4* (8), 1790−1805.
(34) Mott, N. F.; Gurney, R. W.*Electronic Processes in Ionic Crystals*; Clarendon Press: Oxford, U.K. , 1948.
(35) Leighton, P. A. Electronic Processes in Ionic Crystals (Mott, N. F.; Gurney, R. W.). *J. Chem. Educ.* **1941**, *18* (5), 249.
(36) Ho, C. H. Y.; Dong, Q.; Yin, H.; Leung, W. W. K.; Yang, Q.; Lee, H. K. H.; Tsang, S. W.; So, S. K. Impact of Solvent Additive on Carrier Transport in Polymer:Fullerene Bulk Heterojunction Photovoltaic Cells. *Adv. Mater. Interfaces* **2015**, *2* (12), 1500166.
(37) Chan, K. K. H.; Tsang, S. W.; Lee, H. K. H.; So, F.; So, S. K. Charge Transport Study of Semiconducting Polymers and Their Bulk Heterojunction Blends by Capacitance Measurements. *J. Polym. Sci., Part B: Polym. Phys.* **2013**, *51* (8), 649−658.
(38) Tsang, S. W.; So, S. K.; Xu, J. B. Application of Admittance Spectroscopy to Evaluate Carrier Mobility in Organic Charge Transport Materials. *J. Appl. Phys.* **2006**, *99* (1), 013706.
(39) Tsung, K. K.; So, S. K. Advantages of Admittance Spectroscopy over Time-of-Flight Technique for Studying Dispersive Charge Transport in an Organic Semiconductor. *J. Appl. Phys.* **2009**, *106* (8), 083710.
(40) Duan, C.; Huang, F.; Cao, Y. Solution Processed Thick Film Organic Solar Cells. *Polym. Chem.* **2015**, *6* (47), 8081−8098.
(41) Firdaus, Y.; Ho, C. H. Y.; Lin, Y.; Yengel, E.; Le Corre, V. M.; Nugraha, M. I.; Yarali, E.; So, F.; Anthopoulos, T. D. Efficient Double- and Triple-Junction Nonfullerene Organic Photovoltaics and Design Guidelines for Optimal Cell Performance. *ACS Energy Lett.* **2020**, *5* (12), 3692−3701.
(42) Yin, H.; Bi, P.; Cheung, S. H.; Cheng, W. L.; Chiu, K. L.; Ho, C. H. Y.; Li, H. W.; Tsang, S. W.; Hao, X.; So, S. K. Balanced Electric Field Dependent Mobilities: A Key to Access High Fill Factors in Organic Bulk Heterojunction Solar Cells. *Sol. RRL* **2018**, *2* (4), 1700239.
(43) Hosseini, S. M.; Roland, S.; Kurpiers, J.; Chen, Z.; Zhang, K.; Huang, F.; Armin, A.; Neher, D.; Shoaee, S. Impact of Bimolecular Recombination on the Fill Factor of Fullerene and Nonfullerene-Based Solar Cells: A Comparative Study of Charge Generation and Extraction. *J. Phys. Chem. C* **2019**, *123* (11), 6823−6830.
(44) Koster, L. J. A.; Kemerink, M.; Wienk, M. M.; Maturová, K.; Janssen, R. A. J. Quantifying Bimolecular Recombination Losses in Organic Bulk Heterojunction Solar Cells. *Adv. Mater.* **2011**, *23* (14), 1670−1674.
(45) Gupta, V.; Kyaw, A. K. K.; Wang, D. H.; Chand, S.; Bazan, G. C.; Heeger, A. J. Barium: An Efficient Cathode Layer for Bulk-Heterojunction Solar Cells. *Sci. Rep.* **2013**, *3* (1), 1965.
(46) Koster, L. J. A.; Mihailetchi, V. D.; Ramaker, R.; Blom, P. W. M. Light Intensity Dependence of Open-Circuit Voltage of Polymer:-Fullerene Solar Cells. *Appl. Phys. Lett.* **2005**, *86* (12), 123509.
(47) Cowan, S. R.; Roy, A.; Heeger, A. J. Recombination in Polymer-Fullerene Bulk Heterojunction Solar Cells. *Phys. Rev. B* **2010**, *82* (24), 245207.
(48) Würfel, U.; Perdigón-Toro, L.; Kurpiers, J.; Wolff, C. M.; Caprioglio, P.; Rech, J. J.; Zhu, J.; Zhan, X.; You, W.; Shoaee, S.; Neher, D.; Stolterfoht, M. Recombination between Photogenerated and Electrode-Induced Charges Dominates the Fill Factor Losses in Optimized Organic Solar Cells. *J. Phys. Chem. Lett.* **2019**, *10* (12), 3473−3480.
(49) So, S. K.; Chan, M. H.; Leung, L. M. Photothermal Deflection Spectroscopy of Polymer Thin Films. *Appl. Phys. A Mater. Sci. Process.* **1995**, *61* (2), 159−161.
(50) Kuik, M.; Vandenbergh, J.; Goris, L.; Begemann, E. J.; Lutsen, L.; Vanderzande, D. J. M.; Manca, J. V.; Blom, P. W. M. Optical Detection of Deep Electron Traps in Poly(p -Phenylene Vinylene) Light-Emitting Diodes. *Appl. Phys. Lett.* **2011**, *99* (18), 183305.
(51) Chan, M. H.; So, S. K.; Cheah, K. W. Optical Absorption of Free-standing Porous Silicon Films. *J. Appl. Phys.* **1996**, *79* (6), 3273−3275.
(52) Jackson, W. B.; Amer, N. M.; Boccara, A. C.; Fournier, D. Photothermal Deflection Spectroscopy and Detection. *Appl. Opt.* **1981**, *20* (8), 1333.
(53) Ho, C. H. Y.; Cheung, S. H.; Li, H.-W.; Chiu, K. L.; Cheng, Y.; Yin, H.; Chan, M. H.; So, F.; Tsang, S.-W.; So, S. K. Using Ultralow Dosages of Electron Acceptor to Reveal the Early Stage Donor-Acceptor Electronic Interactions in Bulk Heterojunction Blends. *Adv. Energy Mater.* **2017**, *7* (12), 1602360.
(54) Urbach, F. The Long-Wavelength Edge of Photographic Sensitivity and of the Electronic Absorption of Solids. *Phys. Rev.* **1953**, *92* (5), 1324−1324.

https://doi.org/10.1021/acsami.2c11265
ACS Appl. Mater. Interfaces 2022, 14, 47961−47970

(55) Carr, J. A.; Chaudhary, S. The Identification, Characterization and Mitigation of Defect States in Organic Photovoltaic Devices: A Review and Outlook. *Energy Environ. Sci.* **2013**, *6* (12), 3414.
(56) Zhang, C.; Mahadevan, S.; Yuan, J.; Ho, J. K. W.; Gao, Y.; Liu, W.; Zhong, H.; Yan, H.; Zou, Y.; Tsang, S.-W.; So, S. K. Unraveling Urbach Tail Effects in High-Performance Organic Photovoltaics: Dynamic vs Static Disorder. *ACS Energy Lett.* **2022**, *7* (6), 1971−1979.
(57) Ng, A.; Ren, Z.; Hu, H.; Fong, P. W. K.; Shen, Q.; Cheung, S. H.; Qin, P.; Lee, J.-W.; Djurišić, A. B.; So, S. K.; Li, G.; Yang, Y.; Surya, C. A Cryogenic Process for Antisolvent-Free High-Performance Perovskite Solar Cells. *Adv. Mater.* **2018**, *30* (44), 1804402.
(58) Zhang, Z.; Li, Y.; Cai, G.; Zhang, Y.; Lu, X.; Lin, Y. Selenium Heterocyclic Electron Acceptor with Small Urbach Energy for As-Cast High-Performance Organic Solar Cells. *J. Am. Chem. Soc.* **2020**, *142* (44), 18741−18745.
(59) Ghasemi, M.; Ye, L.; Zhang, Q.; Yan, L.; Kim, J.-H.; Awartani, O.; You, W.; Gadisa, A.; Ade, H. Panchromatic Sequentially Cast Ternary Polymer Solar Cells. *Adv. Mater.* **2017**, *29* (4), 1604603.
(60) Ye, L.; Hu, H.; Ghasemi, M.; Wang, T.; Collins, B. A.; Kim, J.-H.; Jiang, K.; Carpenter, J. H.; Li, H.; Li, Z.; McAfee, T.; Zhao, J.; Chen, X.; Lai, J. L. Y.; Ma, T.; Bredas, J.-L.; Yan, H.; Ade, H. Quantitative Relations between Interaction Parameter, Miscibility and Function in Organic Solar Cells. *Nat. Mater.* **2018**, *17* (3), 253−260.
(61) Qin, Y.; Balar, N.; Peng, Z.; Gadisa, A.; Angunawela, I.; Bagui, A.; Kashani, S.; Hou, J.; Ade, H. The Performance-Stability Conundrum of BTP-Based Organic Solar Cells. *Joule* **2021**, *5* (8), 2129−2147.
(62) Szymanski, R.; Henry, R.; Stuard, S.; Vongsaysy, U.; Courtel, S.; Vellutini, L.; Bertrand, M.; Ade, H.; Chambon, S.; Wantz, G. Balanced Charge Transport Optimizes Industry-Relevant Ternary Polymer Solar Cells. *Sol. RRL* **2020**, *4* (11), 2000538.

Recommended by ACS

Synchronous Doping Effects of Cathode Interlayers on Efficient Organic Solar Cells
Zhihui Chen, Yao Liu, *et al.*
OCTOBER 21, 2022
ACS ENERGY LETTERS
READ

Novel Dark Current Reduction Strategy via Deep Bulk Traps for High-Performance Solution-Processed Organic Photodetectors
Hui Lin, Silu Tao, *et al.*
JULY 21, 2022
ACS APPLIED MATERIALS & INTERFACES
READ

Unraveling the Origin of Dark Current in Organic Bulk Heterojunction Photodiodes for Achieving High Near-Infrared Detectivity
Enoch Go, Hae Jung Son, *et al.*
MAY 16, 2022
ACS PHOTONICS
READ

Air-Processable and Thermally Stable Hole Transport Layer for Non-Fullerene Organic Solar Cells
Jules Bertrandie, Derya Baran, *et al.*
JANUARY 10, 2022
ACS APPLIED ENERGY MATERIALS
READ

Get More Suggestions >

https://doi.org/10.1021/acsami.2c11265
ACS Appl. Mater. Interfaces 2022, 14, 47961−47970